



HAL
open science

3D homogenised strength criterion for masonry: application to drystone retaining walls

Hong Hanh Le, Denis Garnier, Anne Sophie Colas, Benjamin Terrade, Jean
Claude Morel

► **To cite this version:**

Hong Hanh Le, Denis Garnier, Anne Sophie Colas, Benjamin Terrade, Jean Claude Morel. 3D homogenised strength criterion for masonry: application to drystone retaining walls. Journal of the Mechanics and Physics of Solids, 2016, 95, pp 239-253. 10.1016/j.jmps.2016.05.021 . hal-01366755

HAL Id: hal-01366755

<https://hal.science/hal-01366755v1>

Submitted on 16 Dec 2024

HAL is a multi-disciplinary open access archive for the deposit and dissemination of scientific research documents, whether they are published or not. The documents may come from teaching and research institutions in France or abroad, or from public or private research centers.

L'archive ouverte pluridisciplinaire **HAL**, est destinée au dépôt et à la diffusion de documents scientifiques de niveau recherche, publiés ou non, émanant des établissements d'enseignement et de recherche français ou étrangers, des laboratoires publics ou privés.

3D homogenised strength criterion for masonry: application to drystone retaining walls

Le, HH, Garnier, D, Colas, A-S, Terrade, B & Morel, J-C

Author post-print (accepted) deposited by Coventry University's Repository

Original citation & hyperlink:

Le, HH, Garnier, D, Colas, A-S, Terrade, B & Morel, J-C 2016, '3D homogenised strength criterion for masonry: application to drystone retaining walls' *Journal of the Mechanics and Physics of Solids*, vol 95, pp. 239-253.

<https://dx.doi.org/10.1016/j.jmps.2016.05.021>

DOI 10.1016/j.jmps.2016.05.021

ISSN 0022-5096

Publisher: Elsevier

NOTICE: this is the author's version of a work that was accepted for publication in Journal of the Mechanics and Physics of Solids. Changes resulting from the publishing process, such as peer review, editing, corrections, structural formatting, and other quality control mechanisms may not be reflected in this document. Changes may have been made to this work since it was submitted for publication. A definitive version was subsequently published in Journal of the Mechanics and Physics of Solids, [95, (2016)] DOI: 10.1016/j.jmps.2016.05.021

© 2016, Elsevier. Licensed under the Creative Commons Attribution-NonCommercial-NoDerivatives 4.0 International

<http://creativecommons.org/licenses/by-nc-nd/4.0/>

Copyright © and Moral Rights are retained by the author(s) and/ or other copyright owners. A copy can be downloaded for personal non-commercial research or study, without prior permission or charge. This item cannot be reproduced or quoted extensively from without first obtaining permission in writing from the copyright holder(s). The content must not be changed in any way or sold commercially in any format or medium without the formal permission of the copyright holders.

This document is the author's post-print version, incorporating any revisions agreed during the peer-review process. Some differences between the published version and this version may remain and you are advised to consult the published version if you wish to cite from it.

3D homogenised strength criterion for masonry: application to drystone retaining walls

Hong Hanh Le^{a,1}, Denis Garnier^b, Anne-Sophie Colas^{c,*}, Benjamin Terrade^c, Jean-Claude Morel^a

^a*Université de Lyon, Laboratoire Génie Civil et Bâtiment, LTDS (UMR 5513), ENTPE, 3 rue Maurice Audin, 69518 Vaulx-en-Velin, France.*

^b*Université Paris-Est, Laboratoire Navier (UMR 8205), ENPC, IFSTTAR, CNRS, 6-8 avenue Blaise Pascal, 77455 Marne-la-Vallée, France.*

^c*Université Paris-Est, MAST, SDOA, IFSTTAR, 14-20 boulevard Newton, 77447 Marne-la-Vallée, France.*

Abstract

A 3D strength criterion for masonry is constructed based on yield design theory. Yield design homogenisation provides a rigorous theoretical framework to determine the yield strength properties of a periodic medium, based on the properties of its constituent materials. First, theoretical basis of 2D homogenisation of periodic media, and more particularly its application in the framework of yield design, will be retrieved. Then, 2D principles are extended to exhibit a 3D domain of running-bond masonry. This criterion is finally used to assess the stability of a drystone retaining wall loaded by an axle load, and theoretical results are compared to experimental data. Perspectives on this work are given as a conclusion.

Keywords: masonry, homogenisation, strength criterion, drystone, retaining wall

*Corresponding author

¹Present address: Faculty of Civil Engineering, National University of Civil Engineering, 59 Giai Phong Street, Hanoi, Vietnam.

1 **1. Introduction**

2 Structural analysis of historical constructions has received a growing at-
3 tention over the past decades, due to the necessary preservation of its her-
4 itage. Actually, the development of modelling proves challenging, considering
5 the strong heterogeneity of the masonry and the diversity of its constitutive
6 materials and patterns.

7 Considering the relative periodicity of their pattern, masonry can be
8 treated as periodic composite media, and homogenisation techniques can be
9 applied in order to derive its mechanical characteristics at macro-scale from
10 the properties of its constituent materials. Pande et al. (1989) pioneered
11 this technique on masonry, in order to evaluate its equivalent modulus of
12 elasticity. This work has been extended later on by Anthoine (1995), on a
13 3D finite thickness pattern. Homogenisation techniques have then been ex-
14 tensively used to assess elastic properties (Cecchi and K., 2002; Cecchi and
15 Sab, 2002; Mistler et al., 2007), or in the framework of limit analysis (Milani
16 et al., 2006a,b; Milani, 2008; Milani and Lourenço, 2010) and finite element
17 analysis (Zucchini and Lourenço, 2002, 2004, 2009).

18 In 1997, de Buhan and de Felice propose an homogenisation approach
19 for masonry developed in the framework of yield design theory. Yield design
20 homogenisation is a rigorous theoretical approach to determine the yield
21 strength properties of a periodic medium, based on the properties of its
22 constituent materials. Extending on this work, the present article introduces
23 a 3D macroscopic strength criterion for running-bond masonry, derived from
24 the strength characteristics of blocks and joints.

25 First, theoretical basis of 2D homogenisation of periodic media, and more
26 particularly its application in the framework of yield design, will be retrieved.
27 This theory is then extended to the three-dimensional case, in order to exhibit
28 a 3D macroscopic strength domain of running-bond masonry. An application
29 of this work is finally given: the 3D strength criterion is used to assess the
30 stability of drystone retaining wall loaded by an axle load in the framework
31 of yield design, and theoretical results given by the model are compared to
32 experimental data. Perspectives on this work are given as a conclusion.

33 **2. Presentation of 2D homogenisation of periodic media principles**

34 Homogenisation of period media consists in replacing the heterogeneous
35 periodic medium by an equivalent homogeneous medium, which macroscopic
36 mechanical properties are derived from the microscopic properties of the orig-
37 inal heterogeneous medium. Introduced by Suquet (1983) in the framework
38 of limit analysis, homogenisation technique has been extended on for yield
39 design analysis of reinforced soils (de Buhan and Salençon, 1990), fibre com-
40 posite materials (de Buhan and Taliercio, 1991), jointed rock mass (Bekaert
41 and Maghous, 1996), and also masonry (de Buhan and de Felice, 1997).

42 Considering a heterogeneous periodic medium, a basic cell V can be iden-
43 tified as the smallest representative volume of material. For every point \underline{x}
44 of V , a microscopic strength domain $G(\underline{x})$ can be defined as the set of ad-
45 missible stress fields $\underline{\underline{\sigma}}(\underline{x})$. Yield design homogenisation aims at defining the
46 macroscopic strength domain G^{hom} of an equivalent homogeneous medium.

47 *2.1. Static definition of G^{hom}*

A static definition of the macroscopic strength domain G^{hom} can be given as the set of admissible macroscopic stress fields $\underline{\underline{\Sigma}}$:

$$G^{\text{hom}} = \left\{ \begin{array}{l} \underline{\underline{\Sigma}} = \langle \underline{\underline{\sigma}}(\underline{x}) \rangle = \frac{1}{V} \int_V \underline{\underline{\sigma}}(\underline{x}) \, dV \end{array} \right. \quad (1a)$$

$$\text{div } \underline{\underline{\sigma}}(\underline{x}) = \underline{\underline{0}} \quad (1b)$$

$$\underline{\underline{\sigma}}(\underline{x}) \cdot \underline{n}(\underline{x}) \text{ antiperiodic } (\underline{n} \text{ unit normal oriented outward}) \quad (1c)$$

$$\underline{\underline{\sigma}}(\underline{x}) \in G(\underline{x}) \quad \forall \underline{x} \in V \quad \left. \vphantom{\int_V} \right\} \quad (1d)$$

48 *2.2. Kinematic definition of G^{hom}*

49 A kinematic definition of the macroscopic strength domain G^{hom} can be
50 given as the set of admissible macroscopic stress fields $\underline{\underline{\Sigma}}$:

$$G^{\text{hom}} = \left\{ \underline{\underline{\Sigma}} / \underline{\underline{\Sigma}} : \underline{\underline{D}} \leq \pi^{\text{hom}}(\underline{\underline{D}}) \right\} \quad (2)$$

51 where:

52 • $\underline{\underline{\Sigma}}$ is defined in equation (1a);

53 • $\underline{\underline{D}}$ is the macroscopic strain rate field given by :

$$\underline{\underline{D}} = \langle \underline{\underline{d}}(\underline{x}) \rangle = \frac{1}{2V} \int_V \left(\underline{\underline{\text{grad}}} \underline{v}(\underline{x}) + {}^t \underline{\underline{\text{grad}}} \underline{v}(\underline{x}) \right) \, dV \quad (3)$$

54 • $\pi^{\text{hom}}(\underline{\underline{D}})$ is the support function of G^{hom} defined as:

$$\pi^{\text{hom}}(\underline{\underline{D}}) = \sup_{\underline{\underline{\Sigma}}} \left\{ \underline{\underline{\Sigma}} : \underline{\underline{D}} / \underline{\underline{\Sigma}} \in G^{\text{hom}} \right\} \quad (4)$$

55 Considering the periodicity of the medium, the virtual velocity field $\underline{v}(\underline{x})$
56 is given by:

$$\underline{v}(\underline{x}) = \underline{\underline{F}} \cdot \underline{x} + \underline{u}(\underline{x}) \quad (5)$$

57 where $\underline{\underline{F}}$ is a second order tensor and $\underline{u}(\underline{x})$ a periodic velocity field. The
 58 associated strain rate field $\underline{\underline{d}}$ can thus be written :

$$\underline{\underline{d}} = \underline{\underline{D}} + \underline{\underline{\delta}} \quad (6)$$

59 where $\underline{\underline{D}}$ is the symmetric part of $\underline{\underline{F}}$ and $\underline{\underline{\delta}}$ the strain rate field associated
 60 with \underline{u} .

61 De Buhan and de Felice (1997) assumed that the support function $\pi^{\text{hom}}(\underline{\underline{D}})$
 62 of the macroscopic strength domain G^{hom} can be written depending on the
 63 support function $\pi(\underline{\underline{d}})$ of the microscopic strength domain $G(\underline{x})$:

$$\pi^{\text{hom}}(\underline{\underline{D}}) = \min_{\underline{\underline{d}}} \langle \pi(\underline{\underline{d}}) \rangle \quad (7)$$

64 *2.3. 2D homogenised strength criterion for masonry*

65 The kinematic approach has been used by de Buhan and de Felice (1997)
 66 to determine a strength criterion G^{hom} for running-bond masonry. Masonry
 67 is made of blocks of height a and thickness b , linked by a joint considered
 68 infinitely thin. The basic cell chosen here has a diamond shape (Fig. 1),
 69 made of four pieces of blocks linked by three sections of joint.

70 Block strength properties are considered to be infinite, compared to the
 71 shear strength of the joints. The joints comply with a Mohr-Coulomb strength
 72 criterion:

$$g(\sigma, \tau) = |\tau| + \sigma \tan \varphi - c \leq 0 \quad (8)$$

73 where σ, τ are the normal and shear stress in the joints, φ the friction angle,
 74 and c the cohesion of the joints.

75 This criterion can also be expressed as a support function of the strength

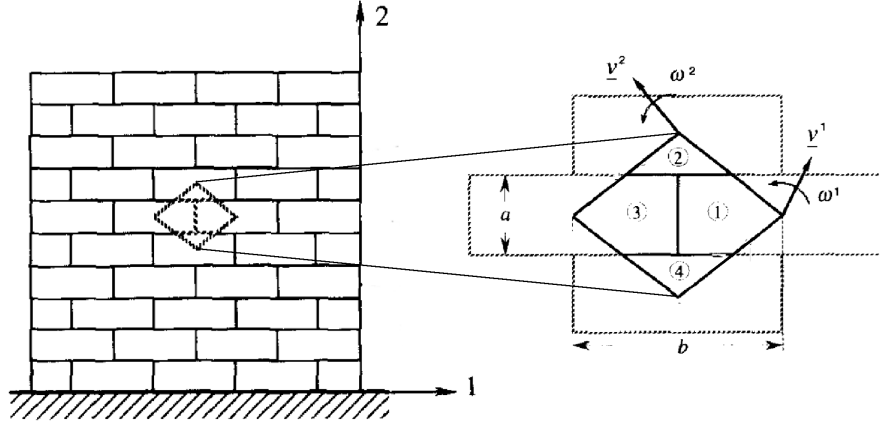


Figure 1: Periodic masonry in 2D, basic cell and rigid block velocity field by de Buhan and de Felice (1997).

76 domain (Salençon, 2013):

$$\pi(\underline{n}, \llbracket \underline{v} \rrbracket) = \begin{cases} \frac{c}{\tan \varphi} \llbracket \underline{v} \rrbracket \cdot \underline{n} & \text{if } \llbracket \underline{v} \rrbracket \cdot \underline{n} \geq \|\llbracket \underline{v} \rrbracket\| \sin \varphi \\ \infty & \text{otherwise} \end{cases} \quad (9)$$

77 The hypothesis of an infinite compressive strength implies that the sup-
78 port function $\pi(\underline{d})$ takes infinite values for $\underline{d} \neq \underline{0}$, implying:

$$\underline{d} = \underline{0} \quad (10)$$

79 Thus, the only relevant velocity fields are rigid body fields, which can be
80 written as:

$$\underline{v}(x) = \underline{v}^i + \omega^i \underline{e}_3 \wedge (x - \underline{x}^i) \quad (11)$$

81 where \underline{v}^i is the translation velocity, ω^i the angular velocity, and \underline{x}^i the position
82 of a point in the block i ($i = 1 \dots 4$).

Indeed, Bekaert and Maghous (1996) showed that periodicity conditions imposes $\omega^i = 0$. The velocity fields thus reduce to translations, that can be written as:

$$\underline{v}^1 = -\underline{v}^3 = \underline{\alpha} \quad (12a)$$

$$\underline{v}^2 = -\underline{v}^4 = \underline{\beta} \quad (12b)$$

83 With these velocity fields (12), equation (5) enables the calculation of \underline{F} :

$$\underline{F} = \frac{2}{b} \underline{\alpha} \otimes \underline{e}_1 + \frac{1}{a} \underline{\beta} \otimes \underline{e}_2 \quad (13)$$

84 and equation (6) the calculation of \underline{D} :

$$\underline{D} = \frac{1}{b} \underline{\alpha} \otimes^s \underline{e}_1 + \frac{1}{2a} \underline{\beta} \otimes^s \underline{e}_2 \quad (14)$$

85 where $\underline{u} \otimes^s \underline{v} = \frac{1}{2} (\underline{u} \otimes \underline{v} + \underline{v} \otimes \underline{u})$

86 Yet, the maximum resisting work $\langle \pi(\underline{d}) \rangle$ in the basic cell is given by:

$$\langle \pi(\underline{d}) \rangle = \frac{1}{V} \left(\int_V \pi(\underline{d}) \, dV + \int_S \pi(\underline{n}, \llbracket \underline{v} \rrbracket) \, dS \right) \quad (15)$$

87 Considering (10) and (9), this expression can be simplified to:

$$\langle \pi(\underline{d}) \rangle = \frac{c}{\tan \varphi} \left(\frac{2}{b} \alpha_1 + \frac{1}{a} \beta_2 \right) \quad (16)$$

88 De Buhan and de Felice (1997) prove that, combining (7), (14) and (16),

89 the expression of the support function $\pi^{\text{hom}}(\underline{D})$ is finally given by:

$$\pi^{\text{hom}}(\underline{D}) = \langle \pi(\underline{d}) \rangle = \frac{c}{\tan \varphi} \text{tr}(\underline{D}) \quad (17)$$

provided the relevancy conditions:

$$-D_{11} \leq 0 \quad (18a)$$

$$f D_{11} \leq 2m D_{22} \quad (18b)$$

$$2 |D_{12}| \leq f D_{11} + \frac{1}{f} D_{22} \quad \text{if } 2m < \frac{1}{f} \quad (18c)$$

90 where $f = \tan \varphi$, and $m = a/b$ is the aspect ratio of the blocks.

91 The macroscopic strength domain G^{hom} is thus given by:

$$G^{\text{hom}} = \left\{ \underline{\underline{\Sigma}} / \underline{\underline{\Sigma}} : \underline{\underline{D}} \leq \pi^{\text{hom}}(\underline{\underline{D}}) = \frac{c}{\tan \varphi} \text{tr}(\underline{\underline{D}}) \right\} \quad (19)$$

92 Fig. 2 shows the representation of G^{hom} in the space of stresses. This representation exhibits the anisotropic character of the masonry.

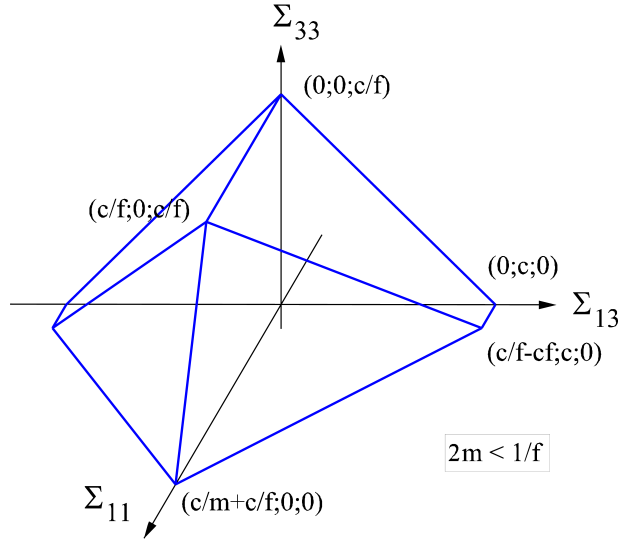


Figure 2: Macroscopic strength domain G^{hom} for running-bond masonry.

93

94 3. Generalisation to 3D homogenised strength criterion for ma- 95 sonry

96 The 2D plane strain approach is here extended on to 3D modelisation.
97 The wall is now considered to be made of blocks of width a , thickness b , and
98 height c , arranged with running bond in the plane of the wall and stack bond

99 out-of-plane (Fig. 3). This pattern has been chosen because it enables an
 analytical resolution of the problem.

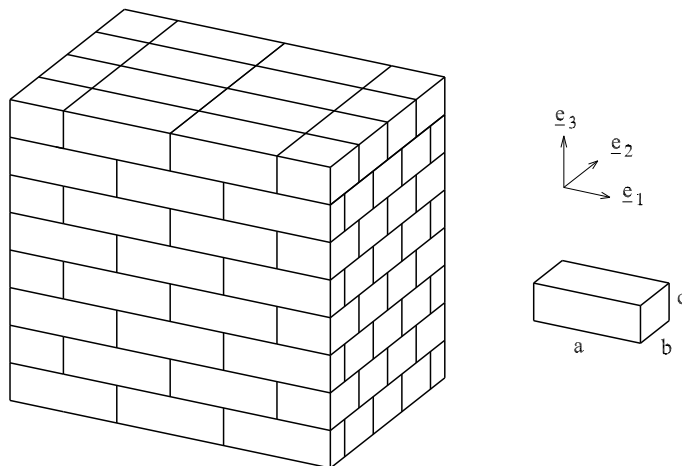


Figure 3: Periodic masonry in 3D.

100

101 The basic cell is a vertical prism (Fig. 4), made of 13 pieces of blocks. It
 102 consists in 3 beds of masonry, and presents a diamond-shape cross-section
 103 in the plane $(\underline{e}_1, \underline{e}_2)$ along beds direction. Indeed, the basic cell is perfectly
 104 symmetric around its centre.

105 Block compressive strength is still considered to be infinite, with zero-
 106 thickness joints complying with a Mohr-Coulomb strength criterion. The
 107 hypothesis of an infinite compressive strength still implies equation (10).
 108 Thus, the only relevant velocity fields are still rigid body fields.

Complying with equation (5) and periodicity conditions, the following
 expressions can be written:

$$\underline{v}_1 - \underline{v}_2 = \underline{\underline{F}} \cdot (2a \underline{e}_1) \quad (20a)$$

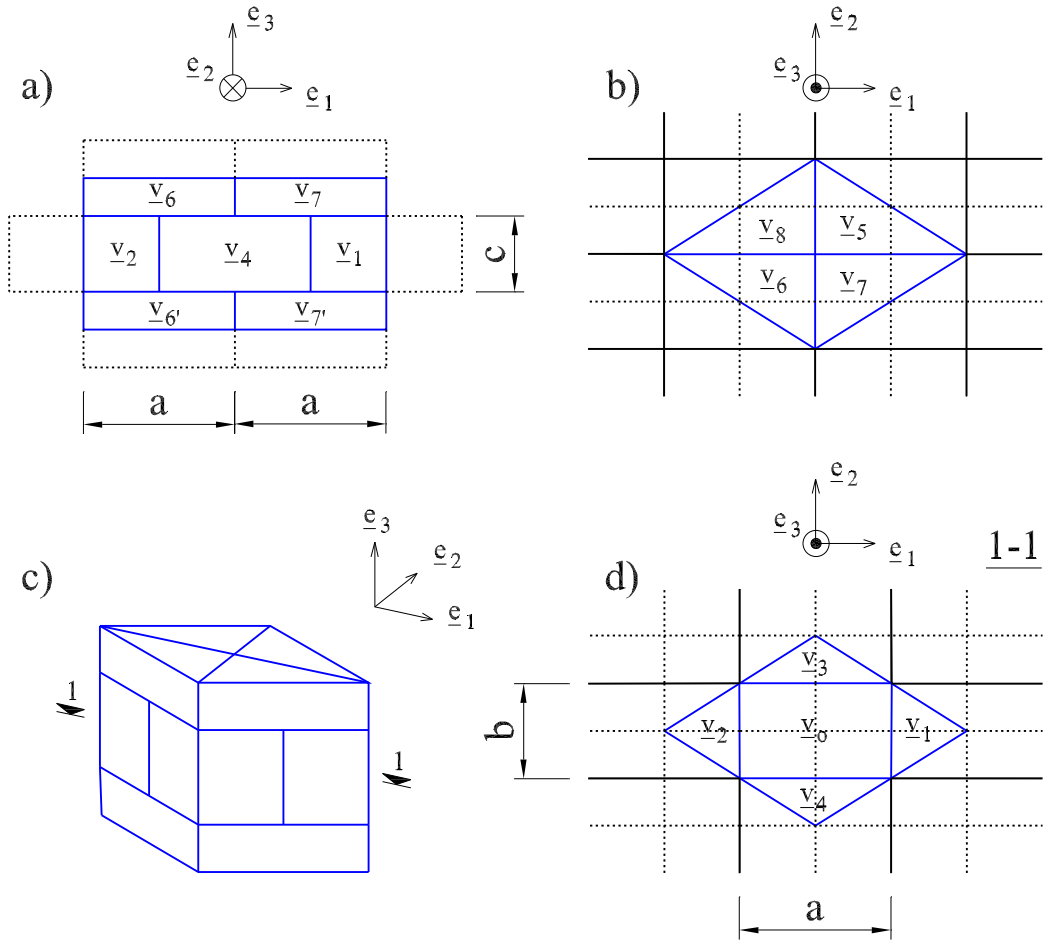


Figure 4: 3D basic cell of masonry.

$$\underline{v}_3 - \underline{v}_4 = \underline{\underline{F}} \cdot (2b \underline{e}_2) \quad (20b)$$

$$\underline{v}_5 - \underline{v}_{5'} = \underline{v}_6 - \underline{v}_{6'} = \underline{v}_7 - \underline{v}_{7'} = \underline{v}_8 - \underline{v}_{8'} = \underline{\underline{F}} \cdot (2c \underline{e}_3) \quad (20c)$$

$$\underline{v}_1 - \underline{v}_4 = \underline{v}_3 - \underline{v}_2 = \underline{v}_5 - \underline{v}_6 = \underline{v}_{5'} + \underline{v}_{6'} = \underline{\underline{F}} \cdot (a \underline{e}_1 + b \underline{e}_2) \quad (20d)$$

$$\underline{v}_7 - \underline{v}_8 = \underline{v}_{7'} + \underline{v}_{8'} = \underline{v}_1 - \underline{v}_3 = \underline{v}_4 - \underline{v}_2 = \underline{\underline{F}} \cdot (a \underline{e}_1 + b \underline{e}_2) \quad (20e)$$

Assuming the velocity of block 0 is null, the following notations can thus

be introduced:

$$\underline{v}_0 = \underline{0} \quad (21a)$$

$$\underline{v}_2 = -\underline{v}_1 = -\underline{\alpha} \quad (21b)$$

$$\underline{v}_4 = \underline{v}_3 = -\underline{\beta} \quad (21c)$$

$$\underline{v}_{5'} = -\underline{v}_6 = -\underline{\varepsilon} + \frac{1}{2}(\underline{\alpha} + \underline{\beta}) \quad (21d)$$

$$\underline{v}_{6'} = -\underline{v}_5 = -\underline{\varepsilon} - \frac{1}{2}(\underline{\alpha} + \underline{\beta}) \quad (21e)$$

$$\underline{v}_{7'} = -\underline{v}_8 = -\underline{\varepsilon} + \frac{1}{2}(\underline{\alpha} - \underline{\beta}) \quad (21f)$$

$$\underline{v}_{8'} = -\underline{v}_7 = -\underline{\varepsilon} - \frac{1}{2}(\underline{\alpha} - \underline{\beta}) \quad (21g)$$

109 With these velocity fields (21), equation (5) enables the calculation of $\underline{\underline{F}}$:

$$\underline{\underline{F}} = \frac{1}{a}\underline{\alpha} \otimes \underline{e}_1 + \frac{1}{b}\underline{\beta} \otimes \underline{e}_2 + \frac{1}{c}\underline{\varepsilon} \otimes \underline{e}_3 \quad (22)$$

110 and the symmetric part of $\underline{\underline{F}}$, represented by the matrix $\underline{\underline{\tilde{D}}}$ in the base

111 $(\underline{e}_1, \underline{e}_2, \underline{e}_3)$:

$$\underline{\underline{\tilde{D}}} = \begin{bmatrix} \frac{\alpha_1}{a} & \frac{1}{2} \left(\frac{\alpha_2}{a} + \frac{\beta_1}{b} \right) & \frac{1}{2} \left(\frac{\alpha_3}{a} + \frac{\varepsilon_1}{c} \right) \\ \frac{1}{2} \left(\frac{\alpha_2}{a} + \frac{\beta_1}{b} \right) & \frac{\beta_2}{b} & \frac{1}{2} \left(\frac{\beta_3}{b} + \frac{\varepsilon_2}{c} \right) \\ \frac{1}{2} \left(\frac{\alpha_3}{a} + \frac{\varepsilon_1}{c} \right) & \frac{1}{2} \left(\frac{\beta_3}{b} + \frac{\varepsilon_2}{c} \right) & \frac{\varepsilon_3}{c} \end{bmatrix}_{(\underline{e}_1, \underline{e}_2, \underline{e}_3)} \quad (23)$$

112 Yet, the maximum resisting work $\langle \pi(\underline{d}) \rangle$ in the basic cell is given by:

$$\langle \pi(\underline{d}) \rangle = \frac{1}{V} \left(\int_V \pi(\underline{d}) \, dV + \int_J \pi(\underline{n}, \llbracket \underline{v} \rrbracket) \, dJ \right) = \frac{c}{\tan \phi} \left(\frac{\alpha_1}{a} + \frac{\beta_2}{b} + \frac{\varepsilon_3}{c} \right) \quad (24)$$

The support function $\pi^{\text{hom}}(\underline{\underline{D}})$ is finally given by (17):

$$\pi^{\text{hom}}(\underline{\underline{D}}) = \frac{c}{\tan \varphi} \text{tr}(\underline{\underline{D}})$$

provided the relevancy conditions:

$$\underline{\alpha} \cdot \underline{e}_1 \geq |\underline{\alpha}| \sin \varphi \quad (25a)$$

$$\underline{\beta} \cdot \underline{e}_2 \geq |\underline{\beta}| \sin \varphi \quad (25b)$$

$$\left(\underline{\varepsilon} + \frac{1}{2}(\underline{\alpha} + \underline{\beta})\right) \cdot \underline{e}_3 \geq \left|\underline{\varepsilon} + \frac{1}{2}(\underline{\alpha} + \underline{\beta})\right| \sin \varphi \quad (25c)$$

$$\left(\underline{\varepsilon} - \frac{1}{2}(\underline{\alpha} + \underline{\beta})\right) \cdot \underline{e}_3 \geq \left|\underline{\varepsilon} - \frac{1}{2}(\underline{\alpha} + \underline{\beta})\right| \sin \varphi \quad (25d)$$

$$\left(\underline{\varepsilon} + \frac{1}{2}(\underline{\alpha} - \underline{\beta})\right) \cdot \underline{e}_3 \geq \left|\underline{\varepsilon} + \frac{1}{2}(\underline{\alpha} - \underline{\beta})\right| \sin \varphi \quad (25e)$$

$$\left(\underline{\varepsilon} - \frac{1}{2}(\underline{\alpha} - \underline{\beta})\right) \cdot \underline{e}_3 \geq \left|\underline{\varepsilon} - \frac{1}{2}(\underline{\alpha} - \underline{\beta})\right| \sin \varphi \quad (25f)$$

113 The macroscopic strength domain G^{hom} is still given by equation (2).

114 It is interesting to note that, considering plane strain conditions, the
115 same results as those given by de Buhan and de Felice (1997) are achieved.

116 In particular, the macroscopic deformation rate (23) becomes:

$$\underline{\underline{\tilde{D}}} = \begin{bmatrix} \frac{\alpha_1}{a} & 0 & \frac{1}{2} \left(\frac{\alpha_3}{a} + \frac{\varepsilon_1}{c} \right) \\ 0 & 0 & 0 \\ \frac{1}{2} \left(\frac{\alpha_3}{a} + \frac{\varepsilon_1}{c} \right) & 0 & \frac{\varepsilon_3}{c} \end{bmatrix}_{(\underline{e}_1, \underline{e}_2, \underline{e}_3)} \quad (26)$$

117 that is plane strain expression recorded in (14). Indeed, G^{hom} is represented
118 by Fig. 2 for plane strain conditions in $(\underline{e}_1, \underline{e}_3)$.

119 4. Application to the stability assessment of drystone retaining 120 walls

121 The three-dimensional strength criterion identified in section 3 is now
122 used to assess the stability of a drystone retaining wall.

123 Drystone walling is an ancient, vernacular form of construction that can
124 be found in many areas around the world. In western Europe, drystone ac-
125 counts for a large part of the retaining walls along road networks. Despite
126 the robustness of these structures, drystone walls are subjected to deterio-
127 ration due to ageing, excessive loading for which they were not designed, or
128 even inappropriate repairs, and there is a growing need for structural anal-
129 ysis methods in order to evaluate their residual bearing capacity. Over the
130 past two decades, advances have been made in France and in the UK for
131 modelling the plane strain behaviour of drystone earth retaining walls. The
132 distinct element method has been extensively used for modelling drystone
133 retaining wall behaviour, more precisely for a better understanding of their
134 pathologies due to ageing (Harkness et al., 2000; Powrie et al., 2002; Clax-
135 ton et al., 2005; Walker et al., 2007). On the other hand, limit equilibrium
136 analyses have been applied to assess the ultimate bearing capacities of these
137 structures (Villemus et al., 2007; Mundell et al., 2009). More recently, this
138 approach has been extended on, using the rigorous framework of yield design
139 (Colas et al., 2010a, 2013). Along with these simulation developments, full-
140 scale experimental campaigns have been undertaken in plane strain (Villemus
141 et al., 2007; Colas et al., 2010b), and 3D (Mundell et al., 2010; McCombie
142 et al., 2012), in order to calibrate and validate the models.

143 Relying on this work, the present paper proposes an innovative 3D mod-

144 elling of these structures. Actually, retaining walls comply with a plane
 145 strain behaviour when they only support their backfill soil but when consid-
 146 ering a traffic loading upon the backfill, a three-dimensional approach should
 147 be adopted. The effects of traffic loadings can be represented by a point load
 148 \underline{F} applied on a rigid plate situated upon the backfill, at a distance d of the
 149 head of the wall, to figure the action of an axle. This study aims to assess
 150 the ultimate load \underline{F}^+ the wall can bear, solely knowing the geometry of the
 151 structure, the loading mode and the strength criterion of the constituent
 152 materials.

153 4.1. Statement of the hypotheses

154 The stability assessment is undertaken in the framework of yield design
 155 theory: the first step consists in identifying the inputs of the model, being
 156 the geometry, loading mode and material strength criterion of the structure.
 157 The geometry and the loading mode are easily described by Fig. 5 and 6.
 158 The strength criteria are detailed below.

159 *Strength criterion of the wall.* The macroscopic strength criterion constructed
 160 in section 3 can be used to characterise drystone, provided the cohesion of
 161 the joints is set to 0. The friction angle φ now represents the friction angle
 162 between the blocks. Expression (2) thus becomes:

$$G^{\text{hom}} = \{ \underline{\underline{\Sigma}} / \underline{\underline{\Sigma}} : \underline{\underline{D}} \leq \pi^{\text{hom}}(\underline{\underline{D}}) = 0 \} \quad (27)$$

163 and the homogenised support function $\pi^{\text{hom}}(\underline{\underline{D}})$:

$$\pi^{\text{hom}}(\underline{\underline{D}}) = 0 \quad (28)$$

164 with respect to the relevancy conditions given by (25).

165 *Strength criterion of the soil.* The backfill soil has been considered as a purely
 166 frictional Mohr-Coulomb soil, where φ_s is the friction angle of the soil. Co-
 167hesion of the soil has been considered as null to simplify calculations and for
 168 safety reasons.

169 The support function and the relevancy conditions of the soil can be found
 170 in Salençon (2013):

$$\pi(\underline{\underline{d}}_s) = 0 \text{ provided } \text{tr } \underline{\underline{d}}_s \geq (|d_{s1}| + |d_{s2}| + |d_{s3}|) \sin \varphi_s \quad (29)$$

$$\pi(\underline{n}_s, \llbracket \underline{v}_s \rrbracket) = 0 \text{ provided } \llbracket \underline{v}_s \rrbracket \cdot \underline{n}_s \geq \|\llbracket \underline{v}_s \rrbracket\| \sin \varphi_s \quad (30)$$

171 where d_{si} are the eigenvalues of the strain rate $\underline{\underline{d}}_s$, and $\llbracket \underline{v}_s \rrbracket$ the velocity
 172 discontinuity across a discontinuity surface of normal \underline{n}_s .

173 *Strength criterion at the soil/structure interaction.* The interface has been
 174 considered as a purely frictional Mohr-Coulomb interface, where δ the fric-
 175tion of the interface equals φ_s the friction angle of the soil. This choice is
 176 motivated by the rough nature of the drystone upstream face, which can
 177 force the failure to occur into the backfill.

178 The support function and the relevancy conditions of the interface can
 179 be found in Salençon (2013):

$$\pi(\underline{n}_\delta, \underline{\Delta v}) = 0 \text{ provided } \underline{\Delta v} \cdot \underline{n}_\delta \geq |\underline{\Delta v} \cdot \underline{t}_\delta| \tan \delta \quad (31)$$

180 where $\underline{\Delta v}$ is the velocity discontinuity at the interface, \underline{n}_δ the normal and \underline{t}_δ
 181 the tangent of the discontinuity surface.

182 Tab. 1 gathers the input parameters of the yield design model.

Table 1: Input parameters of the 3D drystone retaining wall models.

	Symbol	Unit	Definition
Geometry	H	m	Wall height
	l	m	Wall thickness at the top
	f_1	%	Wall batter
	d	m	Distance axle load/top of the wall
	B	m	Half width of the plate
Loading	$\underline{\gamma}$	kN/m ³	Wall unit weight
	$\underline{\gamma}_s$	kN/m ³	Backfill unit weight
	\underline{F}	kN	Axle load
Strength	φ	°	Block friction angle
	φ_s	°	Soil internal friction angle

183 *4.2. Construction of the virtual velocity fields*

184 Fig. 5 and 6 show the velocity field family chosen for this study: it consists
 185 in a translation of a part of the backfill and a translation of part of the wall.
 186 It presents a plane of symmetry (O, \underline{e}_1 , \underline{e}_3). Considering the complexity of
 187 the calculations, it has been decided to restrain to plane failure surfaces.

188 *4.2.1. Velocity field within the wall.*

189 The wall is supposed to fail into 2 parts: a failure zone (JRSTJ'R'S'T'),
 190 which is given a translation velocity \underline{v} , whereas the rest of the wall remains
 191 motionless. The failure zone is delimited by a horizontal surface (JJ'T'T)
 192 at the bottom and two quadrilateral shapes (JRST) and (J'R'S'T') on the

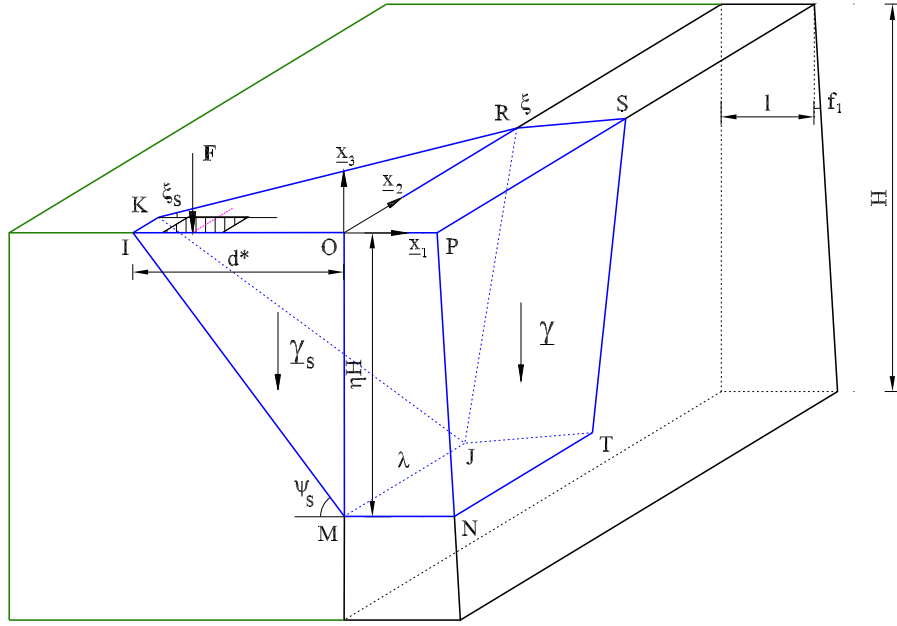


Figure 5: Yield design analysis of a drystone retaining wall subjected to a single axle load: geometry, loading, and velocity fields on a half-system cross-section.

193 edges. The failure zone is bounded by its height ηH , with $\eta \in [0, 1]$, and
 194 the angles ξ and χ respectively between (JRST) or (J'R'S'T') and the axis
 195 \underline{e}_1 and \underline{e}_3 . The surface (JJ'T'T) is taken horizontal because it is the optimal
 196 solution available with analytical calculations.

197 The virtual translation velocity \underline{v} of part (JRSTJ'R'S'T')

$$\underline{v} = V \cos \theta \underline{e}_1 + V \sin \theta \underline{e}_3 \quad (32)$$

198 where θ is the angle between \underline{v} and \underline{e}_1 .

199 This velocity fields has to comply with the relevancy conditions (25) im-
 200 posed by the masonry strength criterion.

201 *Failure surface (JTT'J')*. Considering the macroscopic parameters, the strain
 202 rate $\underline{\underline{D}}$ is given by:

$$\underline{\underline{D}} = \underline{n} \otimes^s [\underline{v}] \quad (33)$$

203 where \underline{v} is given by (32) and $\underline{n} = \underline{e}_3$.

204 Thus:

$$\underline{\underline{\tilde{D}}} = \begin{bmatrix} 0 & 0 & \frac{V}{2} \cos \theta \\ 0 & 0 & 0 \\ \frac{V}{2} \cos \theta & 0 & V \sin \theta \end{bmatrix}_{(\underline{e}_1, \underline{e}_2, \underline{e}_3)} \quad (34)$$

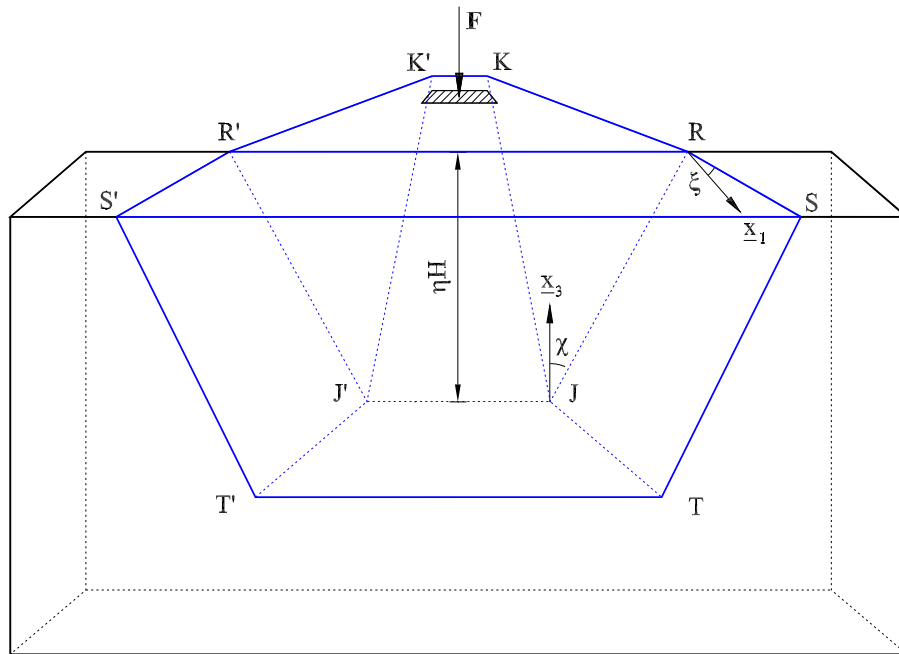


Figure 6: Yield design analysis of a drystone retaining wall subjected to a single axle load: geometry, loading, and velocity fields on a front view.

Yet, $\underline{\underline{D}}$ is also given by (23), using microscopic parameters. Based on (34) and (23), microscopic and macroscopic parameters are thus easily identified:

$$\underline{\alpha} = \underline{\beta} = \underline{0} \quad (35a)$$

$$\varepsilon_1 = cV \cos \theta \quad (35b)$$

$$\varepsilon_2 = 0 \quad (35c)$$

$$\varepsilon_3 = cV \sin \theta \quad (35d)$$

205 Relevancy conditions are finally given by substituting expression given by
206 (35) in (25):

$$\theta \geq \varphi \quad (36)$$

207 *Failure surfaces (JRST) and (J'R'S'T')*. Considering the symmetry of the
208 structure, the calculations will be developed on surface (JRST) only, the
209 expressions for (J'R'S'T') being easily derived.

210 The strain rate $\underline{\underline{D}}$ is still given by (33), with \underline{v} given by (32) and \underline{n} by:

$$\underline{n} = \frac{\tan \xi \underline{e}_1 - \underline{e}_2 + \tan \chi \underline{e}_3}{\sqrt{\tan^2 \xi + 1 + \tan^2 \chi}} \quad (37)$$

211 Thus:

$$\underline{\underline{\tilde{D}}} = \begin{bmatrix} \frac{V \tan \xi \cos \theta}{\sqrt{\tan^2 \xi + 1 + \tan^2 \chi}} & -\frac{V \cos \theta}{2\sqrt{\tan^2 \xi + 1 + \tan^2 \chi}} & \frac{V (\tan \chi \cos \theta + \tan \xi \sin \theta)}{2\sqrt{\tan^2 \xi + 1 + \tan^2 \chi}} \\ -\frac{V \cos \theta}{2\sqrt{\tan^2 \xi + 1 + \tan^2 \chi}} & 0 & -\frac{V \sin \theta}{2\sqrt{\tan^2 \xi + 1 + \tan^2 \chi}} \\ \frac{V (\tan \chi \cos \theta + \tan \xi \sin \theta)}{2\sqrt{\tan^2 \xi + 1 + \tan^2 \chi}} & -\frac{V \sin \theta}{2\sqrt{\tan^2 \xi + 1 + \tan^2 \chi}} & \frac{V \tan \chi \sin \theta}{\sqrt{\tan^2 \xi + 1 + \tan^2 \chi}} \end{bmatrix} \quad (38)$$

Based on the macroscopic (38) and the microscopic (23) definitions of $\underline{\underline{D}}$, microscopic and macroscopic parameters are thus easily identified:

$$\beta_1 = \beta_2 = \beta_3 = 0 \quad (39a)$$

$$\alpha_1 = \frac{aV \tan \xi \cos \theta}{\sqrt{\tan^2 \xi + 1 + \tan^2 \chi}} \quad (39b)$$

$$\alpha_2 = -\frac{aV \cos \theta}{\sqrt{\tan^2 \xi + 1 + \tan^2 \chi}} \quad (39c)$$

$$\varepsilon_2 = -\frac{cV \sin \theta}{\sqrt{\tan^2 \xi + 1 + \tan^2 \chi}} \quad (39d)$$

$$\varepsilon_3 = \frac{cV \tan \chi \sin \theta}{\sqrt{\tan^2 \xi + 1 + \tan^2 \chi}} \quad (39e)$$

$$\frac{\alpha_3}{a} + \frac{\varepsilon_1}{c} = \frac{V(\tan \chi \cos \theta + \tan \xi \sin \theta)}{\sqrt{\tan^2 \xi + 1 + \tan^2 \chi}} \quad (39f)$$

In order to get analytical solutions, the following choices have been made:

$$\alpha_3 = aV \frac{\tan \chi \cos \theta}{\sqrt{\tan^2 \xi + 1 + \tan^2 \chi}} \quad (40a)$$

$$\varepsilon_1 = cV \frac{\tan \xi \sin \theta}{\sqrt{\tan^2 \xi + 1 + \tan^2 \chi}} \quad (40b)$$

212 Relevancy conditions are finally given by substituting expression given by
213 (39) and (40) in (25):

$$\left\{ \begin{array}{l} \varphi \leq \pi/4 \\ \tan \theta \geq a/(2c) \\ \chi = \xi \\ \tan \xi \geq \tan \varphi / \sqrt{1 - \tan^2 \varphi} \end{array} \right. \quad (41)$$

214 Calculations are detailed in Appendix A.

215 4.2.2. Velocity field within the soil

216 The backfill soil is supposed to fail into two parts: a failure zone (KRJJ'R'K'),
217 which is given a translation velocity \underline{v}_s , whereas the rest of the backfill re-

218 mains motionless. The failure zones of the wall and the backfill intersect in
 219 the vertical plane formed by the upper face of the wall, quoted (JRR'J'). The
 220 plane (KJJ'K') forms an angle Ψ_s with \underline{e}_1 , defined by:

$$\tan \Psi_s = \frac{\eta H}{d^*} \tan \Psi_s = \frac{\eta H}{d^*} \quad (42)$$

221 where d^* is the distance between (KK') and (RR').

222 The virtual translation velocity \underline{v}_s of part (KRJJ'R'K') is written:

$$\underline{v}_s = V_s \cos(\psi_s - \varphi_s) \underline{e}_1 - V_s \sin(\psi_s - \varphi_s) \underline{e}_3 \quad (43)$$

223 Considering the velocity field chosen in (43), there is no deformation in
 224 the backfill, thus $\underline{d}_s = \underline{0}$ and $\pi(\underline{d}_s) = 0$. The maximum resisting work of
 225 the backfill is solely governed by the support function (30), provided the
 226 relevancy condition is satisfied. On (KJJ'K'), the condition is fulfilled as the
 227 angle with \underline{v}_s is equal to φ_s . On surface (KRJ), the normal \underline{n}_s is given by:

$$\underline{n}_s = \frac{\tan \xi_s \underline{e}_1 - \underline{e}_2 + \tan \chi \underline{e}_3}{\sqrt{\tan^2 \xi_s + 1 + \tan^2 \chi}} \quad (44)$$

228 with $\tan \xi_s = (\lambda + \eta H \tan \chi - B)/d^*$.

229 The relevancy condition becomes:

$$\frac{\cos(\psi_s - \varphi_s) \tan \xi_s - \sin(\psi_s - \varphi_s) \tan \chi}{\sqrt{\tan^2 \xi_s + 1 + \tan^2 \chi}} \geq \sin \varphi_s \quad (45)$$

230 4.2.3. Velocity jump at the soil/structure interface

231 At the soil/structure interface, the support function is given by (31) and
 232 the relevancy condition becomes:

$$V \geq V_s \frac{\cos(\psi_s - 2\varphi_s)}{\cos(\theta + \varphi_s)} \quad (46)$$

233 4.3. Upper bound axle load

234 The kinematic approach of yield design is based on the application of the
235 principle of virtual works:

$$\forall \underline{v} \text{ kinematically admissible, } W^e \leq W^{\text{mr}} \quad (47)$$

236 which provides an upper bound of the ultimate load \underline{F}^+ .

237 Considering the support function of the wall (28), the soil (30), and the
238 interface (31), the maximum resisting work W^{mr} is given by:

$$W^{\text{mr}} = W_{\text{wall}}^{\text{mr}} + W_{\text{soil}}^{\text{mr}} + W_{\text{interface}}^{\text{mr}} = 0 \quad (48)$$

239 The work of the external forces W^e is given by the sum of the work of
240 the forces in the wall, the soil and due to the axle load F :

$$W^e = W_{\text{wall}}^e + W_{\text{soil}}^e + W_F^e \quad (49)$$

241 The work of the external forces in the wall W_{wall}^e is written:

$$\begin{aligned} W_{\text{wall}}^e &= \int_V \underline{\gamma} \cdot \underline{v} \, dV \\ W_{\text{wall}}^e &= -\gamma V \sin \theta \left[\frac{\eta H}{2} \left(l + \frac{\eta H}{2} f_1 \right) (2\lambda + 2\eta H \tan \chi + 2l \tan \xi + \eta H f_1 \tan \xi) \right] \end{aligned} \quad (50)$$

242 The work of the external forces in the soil W_{soil}^e is written:

$$\begin{aligned} W_{\text{soil}}^e &= \int_V \underline{\gamma}_s \cdot \underline{v}_s \, dV \\ W_{\text{soil}}^e &= \gamma_s V_s \sin(\psi_s - \varphi_s) \left[B d^* \eta H + \frac{1}{3} d^* \eta H (\lambda - B + \eta H \tan \chi) \right] \end{aligned} \quad (51)$$

243 The work of the external forces due to the axle load W_F^e is written:

$$W_F^e = \underline{F} \cdot \underline{v}_F = F V_s \sin(\psi_s - \varphi_s) \quad (52)$$

244 The upper bound inequality (47) leads to:

$$F \leq -\frac{W_{\text{wall}}^e + W_{\text{soil}}^e}{V_s \sin(\psi_s - \varphi_s)} = f(\eta, d^*, \chi, \xi, \lambda, \theta) \quad \forall \eta, d^*, \chi, \xi, \lambda, \theta \quad (53)$$

245 The analytical solution of the upper-bound load F^+ is written depending
246 on input parameters of the problem ($H, l, f_1, d, B, \gamma, \varphi, \gamma_s, \varphi_s$) and kinematic
247 parameters ($\eta, d^*, \chi, \xi, \lambda, \theta$). The upper bound load F^+ is finally given by
248 minimizing function f :

$$F^+ = \min_{\eta, d^*, \chi, \xi, \lambda, \theta} f(\eta, d^*, \chi, \xi, \lambda, \theta) \quad (54)$$

249 with respect to the relevancy conditions (41), (45), and (46)

250 5. Comparison with full-scale experiments

251 The analytical approach performed in section 4 is tested by comparison
252 with experimental results by Mundell et al. (2010) and McCombie et al.
253 (2012). Actually, between 2004 and 2009, the University of Bath has un-
254 dertaken full-scale experiments on drystone retaining walls, aiming at bet-
255 ter understanding the three-dimensional behaviour of these structures, and
256 more particularly the bulge deformation of existing drystone walls. Five ex-
257 perimental drystone walls were built on a moving platform, backfilled by
258 crushed gravel, raised to ensure full frictional interface between the wall and
259 the backfill, and finally loaded by a localised surcharge upon the backfill sur-
260 face, except for wall 1 which was also submitted to tilting of the platform.
261 Wall 1 was built according to standards of drystone construction, whereas
262 walls 2 to 5 were intentionally of poorer construction quality to ensure bulge
263 deformations and failures. Considering the difference of construction and

264 testing protocol of the first test, it has been decided to focus on walls 2 to 5
265 in this study. Geometrical and physical characteristics of the walls, as well
as experimental results are given in Tab. 2.



(a)

(b)

Figure 7: Experimental tests at the University of Bath (Mundell et al., 2010; McCombie et al., 2012): experimental wall (a) and axle load over the backfill (b).

266

267 Considering the specific experimental protocol, with the moving platform,
268 and the poor quality of construction of the walls, the experimental campaign
269 cannot be used directly to validate the model. Yet, it provides a practical
270 framework for a parametric analysis. Thus, the yield design approach previ-
271 ously developed is used to estimate an upper-bound of the ultimate axle load
272 the experimental walls can bear, then compared to the experimental value.
273 The preliminary question which has to be faced with is the choice of the
274 input parameters of the model, and more particularly the aspect ratio of the
275 blocks. Actually, as drystone masonry is made of uncut blocks of different

Table 2: Experimental tests at the University of Bath (Mundell et al., 2010; McCombie et al., 2012): geometrical and physical characteristics, and experimental results.

	Wall 2	Wall 3	Wall 4	Wall 5
Type of stone	limestone	limestone	limestone	slate
Wall height (m)	2.5	2.5	2.5	2.5
Backfill height(m)	2.2	2.2	2.2	2.2
Wall top thickness (m)	0.3	0.4	0.4	0.4
Wall base thickness (m)	0.5	0.6	0.7	0.67
Wall batter (%)	0.08	0.08	0.12	0.11
Wall unit weight (kN/m ³)	19.9	16.8	17	19.7
Backfill unit weight (kN/m ³)	13.7	13.7	13.7	13.7
Block friction angle (°)	37.4	37.4	37.4	17.5
Backfill friction angle (°)	39	39	39	39
Distance load/wall (m)	1	1	1	1
Experimental load (kN)	75	80	85	60

size, it proves quite difficult to evaluate this parameter. Yet, aspect ratio is only involved in the calculation of θ , the angle of the translation velocity of the wall \underline{v} with the horizontal \underline{e}_1 , so that:

$$\theta = \max \{ \arctan(a/2c), \varphi \} \quad (55)$$

The influence of this parameter is assessed on wall 5, as slate friction angle is quite low, compared to limestone friction angle. Fig. 8 shows the evolution of the analytical upper-bound load F^+ depending on the aspect ratio a/c . It can be seen that the analytical solution tends to the experimental value as a/c decreases, and even reaches it for $a/c \approx 0.6$. This value seems very low

as the average aspect ratio of slate blocks seems greater than 2.

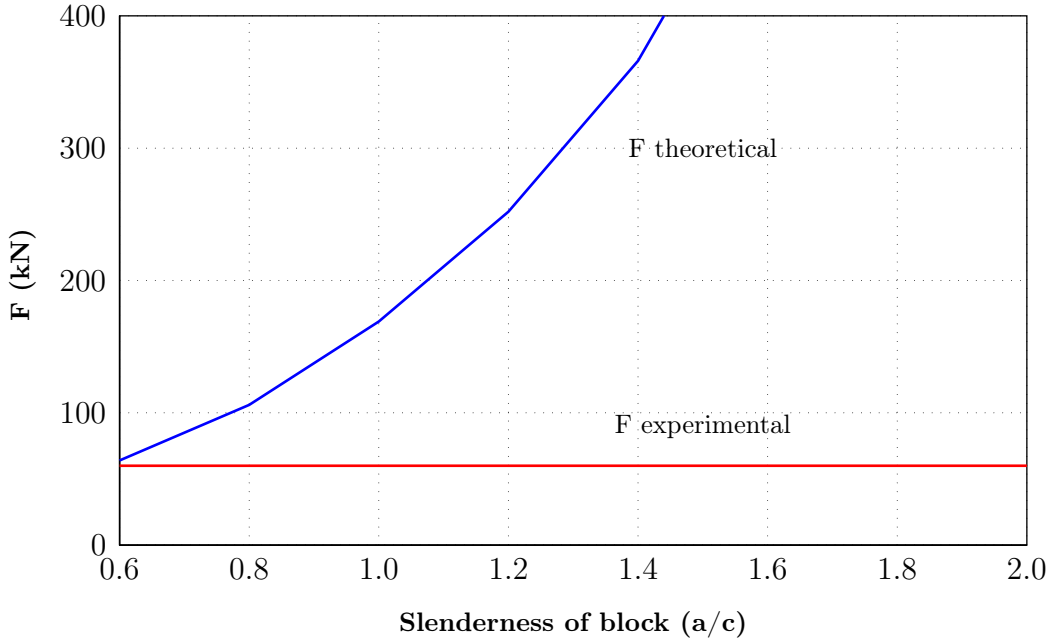


Figure 8: Comparison between theoretical and experimental ultimate load on experiments from the University of Bath, depending on the block aspect ratio a/c .

284

285 Comparing theoretical and experimental upper bound values for F (Fig. 9),
 286 it is worth noting that yield design kinematic approach overestimates the
 287 bearing capacities of drystone experimental walls, which is consistent with
 288 the poor quality of construction of the walls and the upper-bound approach
 289 of the model. With a aspect ratio $a/c = 1$, theoretical values are 6.5 times
 290 greater than experimental results for limestone walls. This can be accounted
 291 for by the relevancy conditions on the macroscopic strength criterion of ma-
 292 sonry, which force the velocity field to form an angle $\theta \geq \varphi$. An additional
 293 possible explanation is the value of the friction angle considered in this study.
 294 Actually, the experimental campaign by Colas et al. (2010a) has showed that

295 the bed joint friction angle in a drystone wall proves about 10° lower than
 296 the block friction angle measured in laboratory. This can be explained by
 297 the internal rotation of the blocks located at the basis of the wall, and by
 298 the difference of contact between wall bed joints and smooth block joints.
 299 Considering a lower friction angle between limestone blocks (27.4° instead of
 300 37.4°), the difference between analytical and experimental solutions vanishes

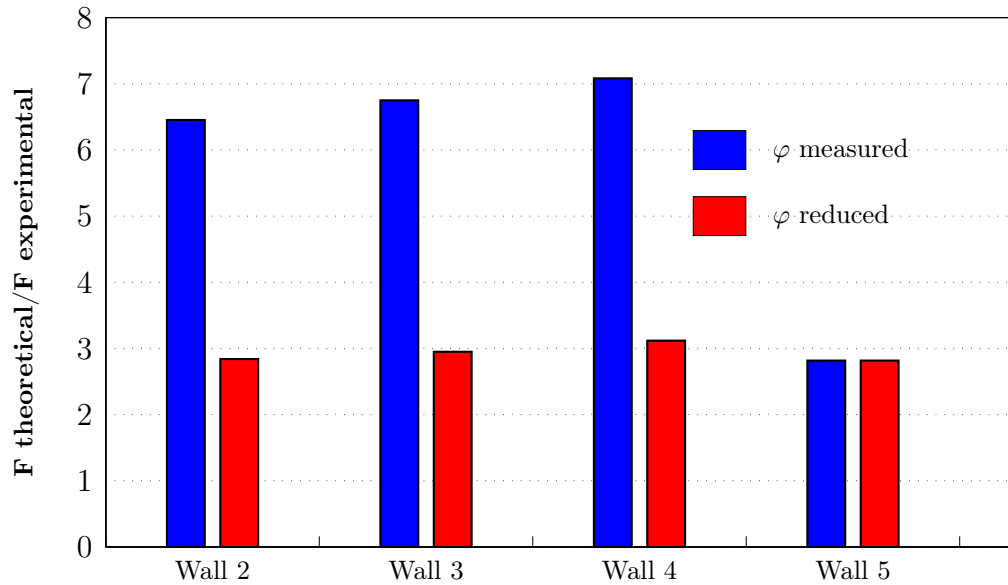


Figure 9: Comparison between theoretical and experimental ultimate load on experiments from the University of Bath (a/c=1)

301

302 The application of the model on an experimental campaign has high-
 303 lighted the importance the block aspect ratio and the block friction angle
 304 on the results, thus enabling a qualitative evaluation of the model. Yet, the
 305 discrepancies between theoretical and experimental values prevent from a

306 quantitative validation. A forthcoming experimental campaign is planned,
307 with experimental walls according to standards of construction and a unique
308 loading mode by a single axle load. This campaign aims to assess the model,
309 and provides additional information on drystone wall 3D behaviour.

310 **6. Conclusion**

311 This paper presents a homogenised 3D strength criterion for masonry.
312 The development of this criterion enables the design and the stability assess-
313 ment of masonry structures in the framework of yield design. An applica-
314 tion is here presented through the stability assessment of drystone retaining
315 walls loaded by a single axle load. Yield design offers a simple but rigorous
316 framework to perform a structural evaluation. Theoretical results are finally
317 compared with experimental results found in the literature: this comparison
318 proves the importance of the input parameters in the model, and more espe-
319 cially the block aspect ratio and the block friction angle. It also highlights the
320 importance of complying experiments with modelling. Perspectives on this
321 work includes greater account taken of the joint friction angle, by distinguish-
322 ing horizontal and vertical joints. Scale down and full-scale experiments will
323 also be planed in order to get experimental results dedicated to the model,
324 thus enabling a better validation of theoretical results.

325 **References**

326 Anthoine, A., 1995. Derivation of the in-plane elastic characteristics of ma-
327 sonry through homogenization theory. *Int J Solids Struct* 32 (2), 137–163.

- 328 Bekaert, A., Maghous, S., 1996. Three-dimensional yield strength properties
329 of jointed rock mass as a homogenized medium. *Mechanics of Cohesive-*
330 *frictional Materials* 1 (1), 1–24.
- 331 Cecchi, A., K., S., 2002. A multi-parameter homogenization study for mod-
332 eling elastic masonry. *Eur J Mech A Solids* 21, 249–268.
- 333 Cecchi, A., Sab, K., 2002. Out of plane model for heterogeneous periodic
334 materials: the case of masonry. *Eur J Mech A Solids* 21 (5), 715–746.
- 335 Claxton, M., Hart, R. A., McCombie, P. F., Walker, P. J., 2005. Rigid block
336 distinct-element modeling of dry-stone retaining walls in plane strain. *J*
337 *Geotech Geoenviron Eng* 131 (3), 381–389.
- 338 Colas, A. S., Morel, J. C., Garnier, D., 2010a. 2D modelling of a dry joint
339 masonry wall retaining a pulverulent backfill. *Int J Numer Anal Methods*
340 *Geomech* 34 (12), 1237–1249.
- 341 Colas, A.-S., Morel, J.-C., Garnier, D., 2010b. Full-scale field trials to assess
342 dry-stone retaining wall stability. *Eng Struct* 32 (5), 1215–1222.
- 343 Colas, A. S., Morel, J. C., Garnier, D., 2013. Assessing the two-dimensional
344 behaviour of drystone retaining walls by full-scale experiments and yield
345 design simulation. *Géotechnique* 63 (2), 107–117.
- 346 de Buhan, P., de Felice, G., 1997. A homogenization approach to the ultimate
347 strength of brick masonry. *J Mech Phys Solids* 45 (7), 1085–1104.
- 348 de Buhan, P., Salençon, J., 1990. Yield strength of reinforced soils as

- 349 anisotropic media. In: Mechanical Engineering Publications. J. P. Boehler,
350 pp. 791–803.
- 351 de Buhan, P., Taliercio, A., 1991. A homogenisation approach to the yield
352 strength of composite materials. *Eur J Mech A Solids* 10 (2), 129–154.
- 353 Harkness, R., Powrie, W., Zhang, X., Brady, K., O’Reilly, M., 2000. Nu-
354 merical modelling of full-scale tests on drystone masonry retaining walls.
355 *Géotechnique* 50 (2), 165–179.
- 356 McCombie, P. F., Mundell, C., Heath, A., Walker, P., 2012. Drystone retain-
357 ing walls: ductile engineering structures with tensile strength. *Eng Struct*
358 45, 238–243.
- 359 Milani, G., 2008. 3D upper bound limit analysis of multi-leaf masonry walls.
360 *Int J Mech Sci* 50 (4), 817–836.
- 361 Milani, G., Lourenço, P. B., Tralli, A., 2006a. Homogenised limit analysis of
362 masonry walls, part I: Failure surfaces. *Comput Struct* 84 (3-4), 166–180.
- 363 Milani, G., Lourenço, P. B., Tralli, A., 2006b. Homogenised limit analysis
364 of masonry walls, part II: Structural examples. *Comput Struct* 84 (3-4),
365 181–195.
- 366 Milani, G., Lourenço, P. B., 2010. A simplified homogenized limit analysis
367 model for randomly assembled blocks out-of-plane loaded. *Comput Struct*
368 88 (11-12), 690–717.
- 369 Mistler, M., Anthoine, A., Butenweg, C., 2007. In-plane and out-of-plane
370 homogenisation of masonry. *Comput Struct* 85 (17-18), 1321–1330.

- 371 Mundell, C., McCombie, P., Bailey, C., Heath, A., Walker, P., 2009. Limit-
372 equilibrium assessment of drystone retaining structures. *Geotech Eng*
373 162 (4), 203–212.
- 374 Mundell, C., McCombie, P. F., Heath, A., Harkness, J., Walker, P., 2010.
375 Behaviour of drystone retaining structures. *Struct Build* 163 (1), 3–12.
- 376 Pande, G. N., Liang, J. X., Middleton, J., 1989. Equivalent elastic moduli
377 for brick masonry. *Comput Geotech* 8, 243–265.
- 378 Powrie, W., Harkness, R., Zhang, X., Bush, D., 2002. Deformation and failure
379 modes of drystone retaining walls. *Géotechnique* 52 (6), 435–446.
- 380 Salençon, J., 2013. *Yield Design*. Wiley-ISTE, London.
- 381 Suquet, P., 1983. Analyse limite et homogénéisation. *C R Acad Sci* 296,
382 1355–1358.
- 383 Villemus, B., Morel, J. C., Boutin, C., 2007. Experimental assessment of
384 dry stone retaining wall stability on a rigid foundation. *Eng Struct* 29 (9),
385 2124–2132.
- 386 Walker, P., McCombie, P., Claxton, M., 2007. Plane strain numerical model
387 for drystone retaining walls. *Geotech Eng* 160 (2), 97–103.
- 388 Zucchini, A., Lourenço, P. B., 2002. A micro-mechanical model for the ho-
389 mogenisation of masonry. *Int J Solids Struct* 39 (12), 3233–3255.
- 390 Zucchini, A., Lourenço, P. B., 2004. A coupled homogenisation-damage
391 model for masonry cracking. *Comput Struct* 82 (11-12), 917–929.

392 Zucchini, A., Lourenço, P. B., 2009. A micro-mechanical homogenisation
 393 model for masonry: Application to shear walls. Int J Solids Struct 46 (3-
 394 4), 871–886.

395 **AppendixA. Determination of the relevancy conditions for the ve-**
 396 **locity field within the wall**

397 The appendix aims at detailing the calculation of relevancy conditions
 398 (41) of the velocity jump on surface (JRST) of the wall.

Based on the macroscopic (38) and the microscopic (23) definitions of $\underline{\underline{D}}$,
 microscopic and macroscopic parameters are thus easily identified:

$$\frac{V \tan \xi \cos \theta}{\sqrt{\tan^2 \xi + 1 + \tan^2 \chi}} = \frac{\alpha_1}{a} \quad (\text{A.1a})$$

$$-\frac{V \cos \theta}{\sqrt{\tan^2 \xi + 1 + \tan^2 \chi}} = \frac{\alpha_2}{a} + \frac{\beta_1}{b} \quad (\text{A.1b})$$

$$\frac{V (\tan \chi \cos \theta + \tan \xi \sin \theta)}{\sqrt{\tan^2 \xi + 1 + \tan^2 \chi}} = \frac{\alpha_3}{a} + \frac{\varepsilon_1}{c} \quad (\text{A.1c})$$

$$0 = \frac{\beta_2}{b} \quad (\text{A.1d})$$

$$-\frac{V \sin \theta}{\sqrt{\tan^2 \xi + 1 + \tan^2 \chi}} = \frac{\beta_3}{b} + \frac{\varepsilon_2}{c} \quad (\text{A.1e})$$

$$\frac{V \tan \chi \sin \theta}{\sqrt{\tan^2 \xi + 1 + \tan^2 \chi}} = \frac{\varepsilon_3}{c} \quad (\text{A.1f})$$

$$(\text{A.1g})$$

399 β_1 and β_3 can be deduced from the introduction of condition (A.1d) in
 400 the microscopic relevancy condition (25b) :

$$\underline{\beta} \cdot \underline{e}_2 = 0 \geq |\underline{\beta}| \sin \varphi \quad \Rightarrow \quad \beta_1 = \beta_2 = \beta_3 = 0 \quad (\text{A.2})$$

The components of the velocity parameters can thus be identified (39):

$$\begin{aligned}
\beta_1 &= \beta_2 = \beta_3 = 0 \\
\alpha_1 &= \frac{aV \tan \xi \cos \theta}{\sqrt{\tan^2 \xi + 1 + \tan^2 \chi}} \\
\alpha_2 &= -\frac{aV \cos \theta}{\sqrt{\tan^2 \xi + 1 + \tan^2 \chi}} \\
\varepsilon_2 &= -\frac{cV \sin \theta}{\sqrt{\tan^2 \xi + 1 + \tan^2 \chi}} \\
\varepsilon_3 &= \frac{cV \tan \chi \sin \theta}{\sqrt{\tan^2 \xi + 1 + \tan^2 \chi}} \\
\frac{\alpha_3}{a} + \frac{\varepsilon_1}{c} &= \frac{V(\tan \chi \cos \theta + \tan \xi \sin \theta)}{\sqrt{\tan^2 \xi + 1 + \tan^2 \chi}}
\end{aligned}$$

In order to get analytical solutions, simplifying choices (40) have been made:

$$\begin{aligned}
\alpha_3 &= aV \frac{\tan \chi \cos \theta}{\sqrt{\tan^2 \xi + 1 + \tan^2 \chi}} \\
\varepsilon_1 &= cV \frac{\tan \xi \sin \theta}{\sqrt{\tan^2 \xi + 1 + \tan^2 \chi}}
\end{aligned}$$

Considering $\underline{\beta} = \underline{0}$ (A.2), the microscopic relevancy conditions vanish to:

$$\underline{\alpha} \cdot \underline{e}_1 \geq |\underline{\alpha}| \sin \varphi \quad (\text{A.3a})$$

$$\left(\underline{\varepsilon} + \frac{1}{2}\underline{\alpha}\right) \cdot \underline{e}_3 \geq \left|\underline{\varepsilon} + \frac{1}{2}\underline{\alpha}\right| \sin \varphi \quad (\text{A.3b})$$

$$\left(\underline{\varepsilon} - \frac{1}{2}\underline{\alpha}\right) \cdot \underline{e}_3 \geq \left|\underline{\varepsilon} - \frac{1}{2}\underline{\alpha}\right| \sin \varphi \quad (\text{A.3c})$$

401 Introducing components α_i and ε_i given by (39) and (40) in (A.3a) boils
402 down to:

$$\begin{aligned}
\alpha_1^2 \cos^2 \varphi &\geq (\alpha_2^2 + \alpha_3^2) \sin^2 \varphi \quad (\text{provided } \cos \theta > 0) \\
\tan^2 \xi \cos^2 \varphi &\geq (1 + \tan^2 \chi) \sin^2 \varphi \\
\tan^2 \xi &\geq (1 + \tan^2 \chi) \tan^2 \varphi
\end{aligned} \quad (\text{A.4})$$

403 Introducing components α_i and ε_i given by (39) and (40) in (A.3b) and
 404 (A.3c) boils down to:

$$\begin{aligned}
 \left(\varepsilon_3 \pm \frac{\alpha_3}{2}\right)^2 \cos^2 \varphi &\geq \left[\left(\varepsilon_1 \pm \frac{\alpha_1}{2}\right)^2 + \left(\varepsilon_2 \pm \frac{\alpha_2}{2}\right)^2 \right] \sin^2 \varphi \\
 \tan^2 \chi \left(c \sin \theta \pm \frac{a}{2} \cos \theta\right)^2 \cos^2 \varphi &\geq \left[(1 + \tan^2 \xi) \left(c \sin \theta \pm \frac{a}{2} \cos \theta\right)^2 \right] \sin^2 \varphi \\
 \tan^2 \chi \cos^2 \varphi &\geq (1 + \tan^2 \xi) \sin^2 \varphi \quad (\text{provided } c \sin \theta > \frac{a}{2} \cos \theta) \\
 \tan^2 \chi &\geq (1 + \tan^2 \xi) \tan^2 \varphi
 \end{aligned} \tag{A.5}$$

405 Combining expressions (A.4) and (A.5), the following conditions can be
 406 written:

$$\left\{ \begin{array}{l} \tan \theta \geq \frac{a}{2c} \\ \tan \chi = \tan \xi \geq \frac{\tan \varphi}{\sqrt{1 - \tan^2 \varphi}} \\ \varphi \leq \frac{\pi}{4} \end{array} \right. \tag{A.6}$$

407 corresponding to the relevancy conditions given in (41).